Oxidation of Hydroxylamine by Nitrous and Nitric Acids. Model Development from First Principle SCRF Calculations

Sumathy Raman,*,†,§ Robert W. Ashcraft,‡ Marc Vial,§ and Marc L. Klasky||

Department of Chemistry, Oakwood College, Huntsville, Alabama 35896, Department of Chemical Engineering, Massachusetts Institute of Technology, Cambridge, Massachusetts 02139, Duke Cogema Stone & Webster, 128 South Tryon Street, Charlotte, North Carolina 28231, and Los Alamos National Laboratory, P.O. Box 1663, MS K575, Los Alamos, New Mexico 8754

Received: June 6, 2005; In Final Form: August 2, 2005

Ab initio molecular orbital calculations have been performed to develop an elementary reaction mechanism for the autocatalytic and scavenging reactions of hydroxylamine in an aqueous nitric acid medium. An improved understanding of the titled reactions is needed to determine the "stability boundary of hydroxylamine" for safe operations of the plutonium−uranium reduction extraction (PUREX) process. Under the operating conditions of the PUREX process, namely, 6 M nitric acid, the reactive forms of hydroxylamine are NH_2OH, NH_3OH^+, and the complex $NH_3OH{\cdot}NO_3$, and those of nitrous acid are NO^+, H_2ONO^+, N_2O_4, N_2O_3, NO_2, and NO. High-level CBSQB3/IEFPCM and CBSQB3/COSMO calculations were performed using GAUSSIAN03 to investigate the energy landscape and to explore a large number of possible ion−ion, ion−radical, ion−molecule, radical−radical, radical−molecule, and molecule−molecule pathways available to the reactive forms of the reactants in solution. It was found that in solution the autocatalytic generation of nitrous acid proceeds through free radical pathways at low-hydroxylamine concentrations from unprotonated NH_2OH via hydrogen abstraction. At high $[NH_3OH^+]$, we suggest a possible involvement of the NH_3ONO^+ intermediate via the reaction $NH_2ONO + NO_2 \rightarrow HNO + HONO + NO$. The NH_3ONO^+ intermediate, in turn, is formed favorably via the ion−ion reactions of NH_3OH^+ with NO^+ and/or the reaction between NO^+ and hydroxylammonium nitrate (HAN). The intermediates involved in the scavenging reaction of nitrous acid by hydroxylamine are NH_3ONO^+, NH_2ONO, $NH_2(NO)O$, NH(NO)OH, and HONNOH and the rate-determining step is the 1,2-NO migration in NH_2ONO leading to $NH_2(NO)O$. Reactions $NH_2ONO \rightarrow NH_2(NO)O$ and $NH_2(NO)O \rightarrow NH(NO)OH$ were studied with two explicit water molecules and the results are discussed in the context of the importance of the explicit treatment of solvent in the determination of the energetics and mechanism of these processes. The rate constants for the reactions were estimated using transition-state theory and other traditional techniques. The kinetic parameters obtained at the B3LYP/CBSB7/IEFPCM level are in reasonable agreement with the limited experimental value. IEFPCM results on free energy of undelocalized polar ions such as NO_3^-, NO_2^-, and NH_3OH^+ are not very accurate and have difficulties in predicting the right direction of acid dissociation equilibrium of $HONO_2$, HONO, and NH_3OH^+. Explicit incorporation of a solvation shell to these ions improves the theoretical descriptions of acid ionization equilibria as it captures some of the nonlocal effects of these ions. Additional work is needed to correctly describe the solvation shell and to introduce consistency in the theoretical treatment involving explicit solvent molecules. Nevertheless, this systematic exploration of reactions in solution and mechanism development for a solution phase process based on self-consistent reaction field (SCRF) results is likely to be one of the first of its kind.

Introduction

Hydroxylamine has been used[1] as a reagent in nuclear fuel reprocessing (PUREX: plutonium−uranium reduction extraction) for the reduction of Pu(IV) to Pu(III) and in the separation of plutonium from uranium in nitric acid solution. Nitrous acid, a powerful catalyst[2] in the reoxidation of Pu(III) to Pu(IV), often coexists in such solutions. Consequently, for many decades, the general chemistry of hydroxylamine in solutions containing nitric and nitrous acids has been a subject of interest. It was found that hydroxylamine can either act as a nitrite scavenger[3−6] (reaction 1) or it may undergo a nitrous acid catalyzed autocatalytic oxidation by nitric acid (reaction 2).[7−9]

$$NH_3OH^+ + HONO \rightarrow N_2O + H_2O + H_3O^+ \quad (1)$$

$$NH_3OH^+ + 2HONO_2 + 2HONO \rightarrow 5HONO + H_3O^+ \quad (2)$$

The global reaction (eq 2) is autocatalytic in the sense that more moles of the reactant HONO are formed as product than initially available, leading to an increased reaction rate as a function of time. However, the presence of nitrous acid is essential for reaction 2, and in its absence, a substantial induction period has been observed experimentally. The autocatalytic exothermic reaction has the potential to generate large amounts of heat and gases. Therefore, it is important to fundamentally understand the reaction mechanism to define safety limits, propose alternative methods for preventing this autocatalytic reaction, and properly design the processing equipment.

* Corresponding author. Department of Chemistry, Oakwood College, Huntsville, AL 35896

† Oakwood College.

‡ Massachusetts Institute of Technology

§ Duke Cogema Stone & Webster.

|| Los Alamos National Laboratory.

10.1021/jp053003c CCC: $30.25
Published on Web 09/07/2005

Different research groups have experimentally investigated the kinetics, mechanism, and stoichiometry of the reaction of hydroxylamine with nitrous and nitric acid in acidic nitrate and perchlorate media. The mechanism of the reaction seems to depend on the ionic strength, and the distribution of products depends on the initial concentration of HONO, NH_3OH^+, and $HONO_2$. Reaction 2 or formation of nitrous acid is reported[7] to be favored by an increase in [$HONO_2$], a decrease in [NH_3OH^+], and an increase in temperature. Stedman[3,4] proposed the mechanism for the scavenging reaction 1 in perchlorate medium with isomerization of O-nitrosated intermediate in (5) as the rate-determining step.

$$HONO + H^+ \rightleftharpoons NO^+ + H_2O \quad (3)$$

$$NO^+ + NH_3OH^+ \rightleftharpoons NH_3ONO^+ + H^+ \quad (4)$$

$$NH_3ONO^+ \rightarrow ONNH_2OH^+ \quad (5)$$

$$ONNH_2OH^+ \rightarrow HONNOH + H^+ \quad (6)$$

$$HONNOH \rightarrow N_2O + H_2O \quad (7)$$

Pembridge and Stedman[8] also suggested a sequence of reaction steps for the autocatalytic process 2. Here, the reaction of N_2O_4 and hydroxylamine, (9), is believed to be the rate-determining step.

$$HONO + H^+ + NO_3^- \underset{\text{equilibrium}}{\overset{\text{rapid}}{\rightleftharpoons}} N_2O_4 + H_2O \quad (8)$$

$$N_2O_4 + NH_2OH \overset{\text{slow}}{\rightleftharpoons} HNO + N_2O_3 + H_2O \quad (9)$$

$$N_2O_4 + HNO \rightarrow HONO + N_2O_3 \quad (10)$$

$$N_2O_3 + H_2O \overset{\text{fast}}{\rightleftharpoons} 2HONO \quad (11)$$

$$NH_3OH^+ \rightleftharpoons NH_2OH + H^+ \quad (12)$$

Although a significant amount of research has been conducted in relation to the PUREX process, the mechanisms proposed to account for the autocatalytic and scavenging reactions are most definitely not elementary; however, they do provide a good starting point for developing a detailed mechanism. Another shortcoming associated with the previous kinetic data is the limited range over which kinetic information was collected. Much of these data fall in the 273−298 K temperature range, whereas the operating temperature of PUREX extraction unit is in the range 313−333 K.

Over the past 2 decades, quantum chemical methods, computer hardware, and rate theory have so improved that one can fairly accurately predict reaction-rate constants for gas-phase reactions a priori, without extensive experimental correlations or qualitative rate-estimation procedures. The goals of this work are to characterize the elementary steps involved in reactions 1 and 2 using quantum chemical methods and to estimate the performance of continuum solvation models in predicting the solution phase thermochemical and kinetic reaction parameters. Since reactions occur in the presence of nitric acid, it is important to consider all possible ionic species and ion−molecule, ion−radical, and ion−ion reactions in addition to free radical reactions in solution.

In aqueous solution, the pK_a of NH_3OH^+ is 5.96 and there is no evidence in the literature for further protonation of NH_3OH^+. Raman spectra[6] of hydroxylammonium nitrate solution did not rule out the possibility of higher-order ion-pair complexes, $NH_3OH{\cdot}NO_3$. The pK_a of HONO is 3.15, suggesting no appreciable concentration of NO_2^- in solution. Consequently, the equilibria of importance for HONO are given in reactions 13−15.

$$2HONO \rightleftharpoons N_2O_3 + H_2O \quad (13)$$

$$HONO + H^+ \rightleftharpoons NO^+ + H_2O \quad (14)$$

$$HONO + HONO_2 \rightleftharpoons N_2O_4 + H_2O \quad (15)$$

For typical acid concentrations employed in the PUREX process, Longstoff and Singer[10] have demonstrated that no appreciable conversion of HONO to NO^+ or N_2O_4 occurs at [$HONO_2$] ≤ 4 M. Hence, the latter two species are postulated to be reactive intermediates. Nitric acid is a very strong acid with a pK_a of −1.44, and at low concentrations it exists predominantly as NO_3^- and H^+ (reaction 16). The calculated concentration of undissociated nitric acid in a 6 M HNO_3 solution based on the pK_a value amounts to 0.93M. Consequently, there is the possibility for undissociated nitric acid to react with H^+ to form NO_2^+ and water. In ordinary nitration reactions, the conventional procedure is to employ a strong acid such as sulfuric acid together with nitric acid for the generation of the electrophile, nitronium ion. Though there is no acid stronger than nitric acid in the mixture, we consider that the concentration of undissociated nitric acid is appreciable for the formation of nitronium ion (reaction 17), another likely reactive intermediate in autocatalytic pathway.

$$HONO_2 \rightleftharpoons H^+ + NO_3^- \quad (16)$$

$$HONO_2 + H^+ \rightleftharpoons NO_2^+ + H_2O \quad (17)$$

N_2O_3 and N_2O_4 formed from reactions of HNO_x have shallow minima in potential energy space and hence relatively low stabilities due to the presence of many lone pairs of electrons. The molecular structure of the higher oxides of nitrogen can be symmetric, viz., ON−O−NO, O_2N-NO_2, or asymmetric, viz., O_2N−NO and O_2N−O−NO, with a weak N−N or N−O bond. Consequently, they exist in rapid equilibrium with the radicals $NO^\bullet$ and $NO_2^\bullet$.

$$N_2O_3 \rightleftharpoons NO + NO_2^\bullet \quad (18)$$

$$N_2O_4 \rightleftharpoons NO_2^\bullet + NO_2^\bullet \quad (19)$$

In the present work, we explore the possible ground-state potential energy surfaces leading to reactions 1 (scavenging) and 2 (autocatalytic) in solution involving the neutral molecules (viz., NH_2OH, NH_3O, HONO, $HONO_2$, N_2O_3, and N_2O_4), cations (viz., NH_3OH^+, NO^+, NO_2^+, $(ON)NH_2OH^+$, $(O_2N)NH_2OH^+$, and $(ONO)NH_2OH^+$), anion (NO_2^-, NO_3^-), free radicals (viz., $NO^\bullet$, $NO_2^\bullet$, $NH_2O^\bullet$, and $OH^\bullet$) and the complex $NH_3OH{\cdot}NO_3$ (HAN). Almost all ionic and neutral species considered in this study have singlet electronic configuration in their ground state except for the radicals that are doublet. Consequently, the molecule−molecule, molecule−ion, ion−ion, and radical−radical reactions are investigated on their singlet surface while molecule-radical and ion−radical have been investigated on their doublet surface. The excited state of interest in this family of molecules is the triplet nπ^* state of the N═O/NO_2 functional group. However, we do not expect any significant contribution from the excited triplet states in the proposed mechanism because of the temperatures at which PUREX process is being performed (313−333 K).

Our goal is to derive necessary thermochemical and kinetic parameters for detailed modeling from quantum chemical

continuum solvation methods coupled with conventional transition-state theory. In the next section, we present the rigorous methodology of deriving them. In the subsequent section we present our thermochemical results in comparison with the existing experimental data, wherever possible. Subsequently, we explore potential energy surfaces leading to the formation of N_2O_4 and N_2O_3, viz., the intermediates suggested in the autocatalytic pathway (reaction 3 and reverse of reaction 7) from reactions between HNO_y's ($y = 3, 2, 1$). Then we discuss pathways for the formation of $NH_3ONO_2^+$ and NH_3ONO^+ intermediates from different forms of hydroxylamine (viz., NH_2-OH, NH_3OH^+, and $NH_3OH.NO_3$) together with NO^+, NO_2^+, $NO^\bullet$, $NO_2^\bullet$, N_2O_4, HONO, and $HONO_2$. The former intermediate is expected to play a key role in the autocatalytic pathway while the latter is important in the scavenging pathway. This section is subsequently followed by the results of our investigations leading to HNO and HONO formation in reaction 2, namely the potential energy surface (PES) corresponding to reactions 9−11. The final results section addresses the reactions of interest in the scavenging reaction 1.

Computational Methodology

Standard ab initio molecular orbital theory calculations were performed using the GAUSSIAN03[11] suite of programs. The geometry of the reactants, products, and transition states (TSs) of the reactions considered in the present study were optimized at the B3LYP/CBSB7 level. CBSB7 is the basis set that can be represented in conventional form as 6-311G(2d,d,p). The energies were calculated using the CBS method, CBSQB3 of Montgomery et al.,[12] which combines the extrapolated CBS second-order limit with higher-order correlation [MP3, MP4, CCSD(T)] energies derived at a relatively smaller basis set for the accurate calculation of molecular energies. The ab initio heats of formation of molecules in gas phase at 298.15 K were obtained from the calculated heat of atomization at 0 K and the experimental heat of formation of atoms using the commonly adopted procedure[13] including corrections[14] for spin−orbit interaction from the energies of the atoms and isodesmic bond additivity corrections.

The solution phase calculations were completed with the IEFPCM model as implemented in GAUSSIAN03 using UAHF radii at the same level of theory. The equilibrium geometry of all neutral and ionic species was optimized at B3LYP/CBSB7 level with the polarized continuum model (PCM) for the solvent using the integral equation formalism approach[15] (IEFPCM). The free energy of the molecule in solution at 0 K is provided by GAUSSIAN03. Thermal corrections were made using the frequencies and moments of inertia of the molecule obtained from the IEFPCM calculation. The total partition function of all species was calculated within the framework of the rigid-rotor−harmonic-oscillator approximation with corrections for internal rotation. The scaled harmonic vibrational frequencies and the moments of inertia were used to calculate the rotational and vibrational partition functions, entropies, and heat capacities. Some low-frequency torsional motions about the single bonds between polyvalent atoms were treated either as a free rotor or as a hindered rotor, depending upon the barrier for the rotor's rotation at the B3LYP/6-31G(d′)/IEFPCM level. The hindrance potential for the internal rotation was obtained by optimizing the $3N - 7$ internal coordinates, except for the dihedral angle, which characterizes the torsional motion. The dihedral angle was varied from 0 to 360° in 30° increments. The potential energy surface thus obtained was then fitted to a Fourier series $\sum_m A_m \cos(m\phi) + B_m \sin(m\phi)$ with $m \leq 8$. The procedure to obtain the hindered rotor partition function associated with this hindrance potential and its thermochemical properties is given in detail in one of our earlier publications.[16] Thermal correction, entropy, and heat capacity $C_p(T)$ were then calculated from the partition function using the statistical machinery. The heat of formation of the molecule in solution is obtained from the gas-phase heat of formation and the enthalpy of solution at 298.15 K.

The rate constant of a reaction A + B → product in solution was calculated based on transition-state theory using the well-known formula

$$k = \frac{\kappa k_B T}{h} \exp\left(\frac{-\Delta G^{\ddagger *}}{k_B T}\right)$$

where $\Delta G^{\ddagger *}$ is the free energy of activation in solution and k_B is the Boltzmann constant. The calculated $k(T)$ was then fitted to the three-parameter Arrhenius expression, $k(T) = AT^n \exp(-E_a/RT)$, for effective use in modeling. The rate constant calculated using transition-state theory does not include tunneling contributions at low temperatures for hydrogen migration reactions. To account for quantum mechanical tunneling effects, we calculated the transmission coefficients, $\kappa(T)$, using the simple Wigner perturbation theory formula[17]

$$\kappa(T) = 1 + \frac{1}{24}\left(1.44\frac{\nu_i}{T}\right)^2$$

where ν_i is the magnitude of the imaginary frequency in reciprocal centimeters corresponding to the reaction coordinate at the transition state and T is the temperature in kelvin.

Results and Discussion

The main problem with the attempt to characterize thermodynamic properties of transition states via ab initio calculations is that there is no direct means to prove the accuracy of the results. Thus, one is left with indirect justifications, such as comparison with results for stable species or verification of theoretically computed reaction rates based on transition-state properties with experimental data. Consequently, we first draw our attention toward the stable species and radicals before dealing with transition-state structures.

Thermochemistry and Proton Affinity of Stable Species. The calculated gas-phase heats of formation in kcal/mol based on CBSQB3 results for NO_x, N_2O_x and HNO_x are compared with experimental values in Table 1 at 298 K. The calculated gas-phase thermochemistry is in good agreement with available experimental values.

Since we will mainly be dealing with cations and anions, it is worthwhile to compare the predictions of CBSQB3 for ionic species. The gas-phase proton affinity (PA) has been measured experimentally for important species such as hydroxylamine and nitric acid. The PA of hydroxylamine was determined[18] earlier by the G1 method to be 194.1 kcal/mol for protonation on nitrogen and 167.5 kcal/mol for protonation on oxygen. The theoretical value found by Angelelli et al.[18] is in excellent agreement with their own experimental value of 194.1 kcal/mol determined by the bracketing method. The values calculated in the present work at CBSQB3 level are 194.8 and 167.8 kcal/mol, respectively, and are in good agreement with earlier data. Ab initio molecular dynamics (MD) simulation[19] of the protonation of nitric acid by a bare proton suggested $NO_2^+ + H_2O$ to be the major product and the proton affinity for the most stable protonated form $NO_2^+(H_2O)$ was found to be 179.9 kcal/mol. At the CBSQB3 level, the calculated proton affinity is 178.7 kcal/mol and the dissociation energy of $NO_2^+(H_2O)$ to

TABLE 1: Comparison of CBSQB3 Calculated Heats of Formation with Experimental Data[28] for the Major Species in Gas Phase[a]

species	CBSQB3 calculated	experimental	species	CBSQB3 calculated	experimental
NO	−26.02	−26.42	NO^+	236.8	NA[b]
NO_2	7.83	7.91	NO_2^+	229.1	NA
NO_3	16.89	17	NO-	21.7	21.66
N_2O	19.61	19.61	NO_2^-	−44.6	−44.2
N_2O_2 (trans)	59.30	NA	NO_3^-	−74.4	−73.2
N_2O_3 ($ONONO_2$)	21.0	NA	HNO	25.37	23.8
N_2O_3 ($ONNO_2$)	20.12	19.8	HONO	−18.33	−18.34
N_2O_4	1.65	2.17	$HONO_2$	−32.15	−32.10
N_2O_5	2.33	2.707	NH_2OH	−11.3	−11.4
NH_2O	14.12	NA	NH_3OH^+	159.17	161.6

[a] Heats of formation are given in kcal/mol. [b] NA stands for nonavailable data.

TABLE 2: Thermochemical Properties Calculated at the B3LYP/CBSB7/IEFPCM Level for the Species Involved in Autocatalytic and Scavenging Reactions of Hydroxylamine

molecules	$\Delta_f H^{298}$	S^{298}	$C_p(T)$ [solution phase values] 300	400	500	600	800	1000	1500
H_2O	−64.23	46.51	8.01	8.17	8.41	8.68	9.26	9.85	11.17
$HONO_2$	−38.06	64.40	13.18	15.38	17.14	18.53	20.49	21.77	23.56
HONO	−23.17	59.33	10.90	12.32	13.46	14.46	15.67	16.58	17.94
NH_2OH	−19.27	57.00	10.82	12.28	13.70	14.96	17.00	18.59	21.33
N_2H_4	12.26	56.09	11.28	13.27	15.23	16.97	19.83	22.07	25.84
NO_3^-	−136.42	60.14	10.78	12.68	14.24	15.42	16.98	17.88	18.92
H_3O^+	32.31	46.38	8.71	9.53	10.40	11.24	12.81	14.15	16.46
HAN	−70.13	89.77	21.68	25.95	29.79	33.05	38.06	41.61	46.83
$NH_3ONO_2^+$	112.79	72.70	17.51	20.91	23.94	26.51	30.48	33.29	37.41
$N_2H_5^+$	95.45	57.43	11.35	13.77	16.25	18.52	22.32	25.30	30.24
$ONONO_2$	9.64	83.94	17.78	20.18	22.05	23.50	25.51	26.75	28.28
O_2NNO_2	3.47	78.70	17.65	20.17	22.18	23.78	26.02	27.41	29.11
NO_2	9.83	57.33	8.85	9.60	10.32	10.94	11.87	12.46	13.19
NH_2O	6.47	55.71	10.09	10.84	11.68	12.48	13.87	14.99	16.89
HNO	22.4	52.73	8.08	8.43	8.92	9.45	10.42	11.20	12.38
ONONO	20.87	75.57	15.72	17.30	18.60	19.67	21.25	22.26	23.54
NO_2^-	−110.28	56.60	8.92	9.82	10.63	11.29	12.19	12.72	13.33
NO^+	157.75	47.32	6.96	6.98	7.04	7.14	7.43	7.72	8.23
NO	25.03	49.02	6.97	7.04	7.19	7.37	7.74	8.03	8.45
NH_3OH	66.32	56.62	10.63	12.63	14.68	16.56	19.69	22.13	26.07
N_2O	18.19	52.49	9.19	10.13	10.87	11.48	12.40	13.03	13.91
t-NH_3ONO^+	120.06	74.40	15.29	17.47	19.58	21.49	24.61	26.96	30.64
t-NH_2ONO	15.62	67.73	15.98	18.18	20.05	21.60	23.95	25.63	28.19
$ONNH_2O$	23.18	67.55	15.66	17.90	19.81	21.39	23.84	35.59	28.24
ONNHOH	1.46	66.98	15.91	18.26	20.25	21.88	24.32	26.01	28.50
$ONNH^+$	171.24	56.45	10.10	11.33	12.32	13.11	14.33	15.29	16.98
NO_2^+	154.53	51.12	8.99	9.91	10.65	11.27	12.22	12.88	13.82
$NH_3OH.H_2O$	7.06	76.66	19.19	21.92	24.59	27.02	31.12	34.40	39.96
NH_2ONO_2	1.11	71.27	18.30	21.37	23.88	25.89	28.82	30.84	33.78
NH_2O^+	132.82	55.12	8.41	9.26	10.33	11.42	13.35	14.84	17.08
HONNOH	−10.51	65.95	16.00	18.45	20.42	21.98	24.25	25.83	28.25
$HONN^+$	163.95	59.04	10.83	12.01	13.02	13.90	15.34	16.41	17.97

[a] $\Delta_f H^{298}$ is in kcal/mol, S^{298} and $C_p(T)$ data are in cal mol^{-1} K^{-1}

nitronium ion is 16.3 kcal/mol. The latter value is in good agreement with the experimentally determined value of 14.8 ± 2.3 kcal/mol by Sunderlin and Squires.[20] There are two distinguishable oxygen sites in nitrous acid: the terminal oxygen site and the central oxygen site. Protonation on the central oxygen yields a loose complex between H_2O and NO^+. The ab initio proton affinity in the gas phase of nitrous acid is 186.6 kcal/mol, and the calculated dissociation energy of $NO^+(H_2O)$ to nitrosonium ion and water is 18.5 kcal/mol.

The experimental gas-phase acidities of $HONO_2$ ($HONO_2 \rightarrow H^+ + NO_3^-$) and HONO ($HONO \rightarrow H^+ + NO_2^-$) can be obtained from the gas-phase heats of formation of the neutrals and the ions and are 324.1 and 339.3 kcal/mol, respectively. The experimental heat of formation of gaseous H^+ ion is 365.2 kcal/mol. The calculated values for the corresponding acidities of 323.5 and 339.5 kcal/mol, respectively, are in good agreement with experimental data.[21] In summary, the thermochemical parameters and gas-phase acidities calculated at the CBSQB3 level for HNO_x species are in good agreement with the available experimental data.

The solution phase thermochemistry of all relevant species considered in the autocatalytic and scavenging pathways has been compiled in Table 2. There are not enough experimental data available for its comparison; however, it is observed that the B3LYP/CBSB7/IEFPCM or CBSQB3/IEFPCM methods do not reproduce the stabilities of ionic species in solution very well. The $\Delta G°$ at 298 K for the acid dissociation of $HONO_2$ is 0.56 kcal/mol, as opposed to −1.96 kcal/mol (from pK_a of −1.44), and for NH_3OH^+ the value is 5.97 kcal/mol instead of 8.13 kcal/mol (from pK_a of 5.96). These errors are most likely caused by the undelocalized and polar nature of the NO_3^- and NH_3OH^+ ions, which in a liquid show nonlocal polarization effects. Explicit consideration of a solvation shell improves the description. However, from a theoretical point of view, such a procedure introduces some degree of arbitrariness into the calculation, because one is not sure about the specific complex

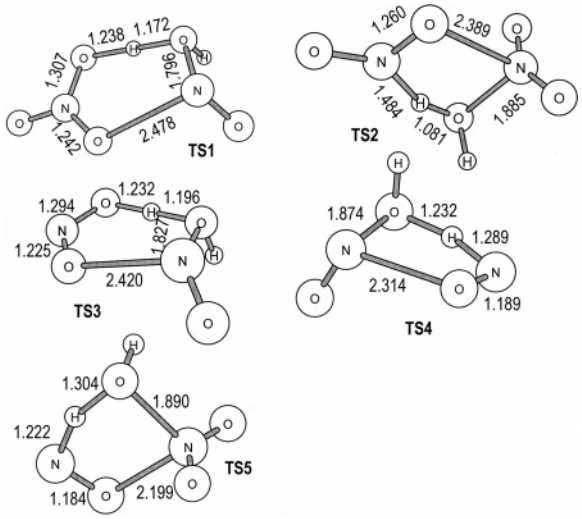

Figure 1. B3LYP/CBSB7/IEFPCM optimized geometries of molecular elimination transition states for the reactions between HNO_y's (y = 1,2,3). The value of bond length along the breaking and forming bonds in the reaction coordinate is given in angstroms.

and the number of solvent molecules that should be included in the solvation shell. Consequently, we do not advocate this approach. A better alternative would be to introduce polarizability corrections to the quantum chemical treatment, but such an approach is not available in any of the existing quantum chemical codes. This under- or overestimation of the stability of ionic species in solution is anticipated to be systematic and is expected to cancel out while calculating the barrier heights involving ionic reactants and transition states.

Formation of N_2O_x (x = 2, 3, 4) from HNO_x (x = 1, 2, 3) Molecular Elimination Reactions. As can be seen from Table 1 and the previous section, the agreement between calculated and measured values for the thermochemistry of stable species is good, and so we continue investigating the potential energy surfaces (both gas phase and solution phase) for the following reactions:

$$HONO + HONO_2 \rightarrow ONONO_2 + H_2O \quad \text{(TS1)} \quad (k_1 \text{ and } k_{-1}) \quad (20)$$

$$HNO_2 + HONO_2 \rightarrow O_2NNO_2 + H_2O \quad \text{(TS2)} \quad (k_2 \text{ and } k_{-2}) \quad (21)$$

$$HONO + HONO \rightarrow ONONO + H_2O \quad \text{(TS3)} \quad (k_3 \text{ and } k_{-3}) \quad (22)$$

$$HONO + HNO \rightarrow N_2O_2 + H_2O \quad \text{(TS4)} \quad (k_4 \text{ and } k_{-4}) \quad (23)$$

$$HONO_2 + HNO \rightarrow H_2O + O_2NNO \quad \text{(TS5)} \quad (k_5 \text{ and } k_{-5}) \quad (24)$$

As listed in the Introduction, N_2O_4 and N_2O_3 are the intermediates in the autocatalytic scheme proposed by Stedman. Herein, we explore their formation rate constants from the corresponding acids. The transition states obtained for these five molecular reactions at the B3LYP/CBSB7/IEFPCM level of theory are presented in Figure 1. All transition states are well-defined. In almost all cases, we found the N−OH bond was almost broken, and the analysis of the eigenvector corresponding to the sole negative eigenvalue of the force constant matrix demonstrates a dominant contribution from the migration of H with this OH group. In Table 3, we list the important characteristics of these transition states, viz., the magnitude of the imaginary frequency (in cm^{-1}) and the barrier heights (in kcal/mol) for the gas phase and solution phase. Also included are the rate constants (cm^3/(mol K)) at 298 K together with the fitted A, n, and E_a/R parameters for the solution phase. These parameters are obtained by fitting $k(T)$ calculated from 298 to 398 K in steps of 5 K.

In general, molecular reactions are less common in solution phase compared with the gas phase and they are expected to proceed slower. Here the reactants are overall neutral, though polar, and the activated complexes are also overall neutral. Qualitatively, existence of charge distributed over the activated complex would encourage solvation. The greater the degree of charge separation in the activated complex, the greater will be the impact of solvation and in turn an increased orientation of the solvent on activation. Consequently, the entropy of activation in solution phase will be decreased compared with its gas-phase values. However, the enthalpy of activation be only slightly affected because of changes in solvation pattern compared with the gas phase. The changes in solvation pattern on activation depend on the degree of charge separation. This would result in slight lowering of $\Delta H^{\ddagger}$ relative to the gas phase.

In regard to the autocatalytic reaction pathways, the kinetics of reactions 20 (k_1 and k_{-1}) and 22 (k_3 and k_{-3}) are very important. They correspond to reactions 8 and the reverse of reaction 11 in the proposed mechanism by Stedman. Schwartz and White[22] have given a comprehensive review of the rate constants of aqueous phase reactions involving nitrogen oxides. The value recommended for k_{-1} is 7×10^7 M^{-1} s^{-1}, with 3.5×10^7 and 1×10^8 as the lower and upper bounds, respectively. Park and Lee[23] measured k_{-1} at 22 °C to be $(8.4 \pm 1.5) \times 10^7$ M^{-1} s^{-1}. It must be stated that [H_2O] is lumped into the rate constant and is not therefore directly comparable with our calculated rate constants. The calculated barrier height for reverse reaction 20 is 4.5 kcal/mol at CBSQB3 level but only 0.9 kcal/mol at B3LYP/CBSB7/IEFPCM level, which suggests a very fast reaction in the order that has been observed in the literature. The forward reaction is less likely to proceed from the neutral $HONO_2$ molecule, as it exists predominantly as H^+ and NO_3^- ions in solution. Even if the rate constant for the molecular reaction were higher, the rate of the reaction will not be appreciable because of a concentration of undissociated $HONO_2$ molecules. Instead it could be a multistep heterogeneous reaction involving fast equilibriums.

$$HONO + H^+ \rightleftharpoons H_2O + NO^+$$

$$HONO_2 \rightleftharpoons H^+ + NO_3^-$$

$$NO^+ + NO_3^- \rightarrow N_2O_4 \text{ (or } 2NO_2^{\bullet})$$

All these reactions proceed on the attractive potential and so they are not characterized by specific transition states and are diffusion limited. The third-order rate constant value (5.0×10^{-3} M^{-2} s^{-1} at 298 K) reported in the literature for k_1 cannot be compared with the second-order transition state theory (TST) estimate. The activation energy reported by Schmid and Bahr[24] for the third-order reaction is 18.3 kcal/mol (as measured by Abel and Schmid[25]) and the Arrhenius plot of this reaction after appropriate correction for nonideality leads to a barrier height of 15.9 kcal/mol.[26] The calculated barrier height for the molecular elementary reaction between HONO and $HONO_2$ is found to be lower (13.3 kcal/mol).

Schwartz and White[22] recommended a value of 5.6 M^{-1} s^{-1} for k_3 at 25 °C. Park and Lee[23] determined a value of 13.4 M^{-1} s^{-1} at 22 °C. Our calculated value of 3.2 M^{-1} s^{-1} is in good agreement with Schwartz estimates. It must be stated that the

TABLE 3: CBSQB3 Calculated Barrier Heights (ZPE Corrected) for the Gas-Phase and B3LYP/CBSB7/IEFPCM Barrier Heights for the Solution Phase, Magnitude of the Imaginary Frequencies, Value of the Rate Constant (cm^3/(mol s)) at 298.15 K, and the Modified Arrhenius-Fitted Parameters for the Reaction in Aqueous Solution

reacn	E_0(gas)	E_0(soln)	ν(gas)	ν(soln)	k(g)(298K)	k(soln)(298K)	A	n	E_a/R
20	10.6	13.3	742*i*	737*i*	1.7E2	1.2E3	4.9E2	2.59	6037
21	31.0	29.7	1019*i*	509*i*	5.4E−13	2.1E−12	6.7E0	3.29	14 220
22	17.3	9.7	1025*i*	1012*i*	5.0E−3	3.2E3	6.5E2	2.58	4106
23	22.2	14.5	1227*i*	1253*i*	1.4E−6	0.66	2.6E1	2.87	6250
24	36.0	30.7	1285*i*	1381*i*	7.0E−16	2.1E−12	6.2E3	2.26	14 450

TABLE 4: CBSQB3 Calculated Barrier Heights (Zero Point Energy (ZPE) Corrected) in Gas-Phase and B3LYP/CBSB7/IEFPCM Barrier Heights in Solution Phase, Magnitude of the Imaginary Frequencies, Value of the Rate Constant (cm^3/(mol s)) at 298.15 K, and the Modified Arrhenius-Fitted Parameters for the Formation of $NH_3ONO_2^+$ and NH_3ONO^+ Intermediates in Aqueous Solution

reacn	E_0(gas)	E_0(soln)	ν(gas)	ν(soln)	k(g)(298K)	k(soln)(298K)	A	n	E_a/R
25	24.3	30.5	559*i*	734*i*	1.4E−6	2.1E−13	0.83E2	2.86	14 880
26	12.3	39.3	143*i*	280*i*	6.2E1	6.5E−19	0.29E5	2.31	19 460
27	3.4	24.1	133*i*	365*i*	8.5E8	2.2E−7	0.33E6	2.04	11 810
28	77.0	95.0	597*i*	803*i*					
29	68.0		614*i*						
30		9.2		350*i*		8.8E3	8.66E4	2.03	4131
31		3.2		334*i*		2.2E9	7.30E6	1.65	1130
32		1.2		816		1.1E10	1.9E4	2.14	168.8
33		1.0		865		1.1E12	9.4E6	1.86	145.5

CBSQB3 barrier for this reaction is ∼5 kcal/mol higher than the B3LYP/CBSB7 barrier and the latter is in good agreement with experimental data. The complete basis set procedure was originally developed and parametrized for gas-phase thermochemistry, and it is understandable if extrapolations using smaller basis sets in the presence of SCRF do not explain the solution phase energetics equally accurately. For the sake of consistency, in our systematic exploration of rate parameters, we adopt the B3LYP/CBSB7/IEFPCM results.

Formation of the Intermediate, $NH_3ONO_2^+$ and NH_3ONO^+. As highlighted in the Introduction, NO^+, NO_2^+, $NO^\bullet$, $NO_2^\bullet$, N_2O_4, and N_2O_3 are the reactive intermediates from nitrous and nitric acid. Consequently, reactions 4 and 9 in the proposed mechanism could proceed through reactions between hydroxylamine and one of these reactive intermediates. Furthermore, as stated earlier in the Introduction, hydroxylamine could exist in the protonated, NH_3OH^+, unprotonated, NH_2OH, or the complexed form, $NH_3OH{\cdot}NO_3$. Consequently, we explored a large number of reactions between hydroxylamine and nitrous/nitric acid and the reactions investigated in this work can be broadly categorized as the following:

(i) Ion−molecule reactions involving hydroxylammonium ion (NH_3OH^+).

(ii) Ion−radical reactions involving hydroxylammonium ion (NH_3OH^+).

(iii) Ion−ion reactions involving hydroxylammonium ion (NH_3OH^+).

(iv) Ion−molecule reactions involving HAN ($NH_3OH{\cdot}NO_3$).

(v) Ion−molecule reactions involving Hydroxylamime (NH_2-OH).

All these reactions were investigated both in the gas phase and in the solution phase at CBSQB3 and B3LYP/CBSB7/IEFPCM levels. The calculated barrier heights (Table 4) differ significantly between the two phases. Before discussing the results, it is worthwhile to review the basics of how a solvent can influence reactions in solutions. The solvent modifies the electrostatic interactions between charges. It reduces the field strength due to the charges, it reduces the forces acting on the charges, and it reduces the potential energy of interaction between the charges. The solvent reduces these quantities by a factor of its relative permittivity, ϵ_r. The solvent restricts the movement of reactants by its viscosity, η. Its polarizability, α, is a measure of the extent to which the electronic distribution over a molecule can be distorted by the electric field of charged particles or dipolar molecules. Consequently, in contrast to gas-phase reactions, reactions involving ions, polar molecules, and charged-transition states occur readily in a solution. In addition, intermediates are at equilibrium concentrations in solution while in gas phase are often found in steady-state concentrations. Often the reaction kinetics in solution is dictated by the diffusion rate rather than the reaction rate, and this is especially the case for fast ionic reactions.

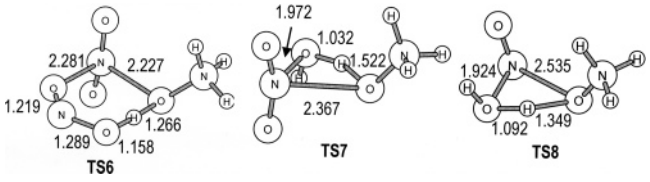

Figure 2. B3LYP/CBSB7/IEFPCM optimized geometries of ion−molecule reactions leading to $NH_3ONO_2^+$ and NH_3ONO^+ intermediates. The value of bond length along the forming and breaking bonds in the reaction coordinate is given in angstroms.

Ion—Molecule Reactions Involving Hydroxylammonium Ion (NH_3OH^+). Here

$$NH_3OH^+ + N_2O_4 \rightarrow NH_3ONO_2^+ + HONO \quad (TS6) \quad (25)$$

$$NH_3OH^+ + HONO_2 \rightarrow NH_3ONO_2^+ + H_2O \quad (TS7) \quad (26)$$

$$NH_3OH^+ + HONO \rightarrow NH_3ONO^+ + H_2O \quad (TS8) \quad (27)$$

The optimized geometries of TS6, TS7, and TS8 are shown in Figure 2. All of them are late-transition states and the eliminating products HONO or H_2O are nearly formed. The reaction coordinate beyond the transition state seems to be the formation of the O−N bond in the intermediate. The barrier heights and fitted-rate parameters for these reactions are tabulated in Table 4. In all these reactions there is a discrete charge on one of the reactants and a dipole on the other. In the thermodynamic formulation of the transition- state theory, the free energy of activation in solution should be equal to the sum of free energy of activation in the gas phase and the electrostatic interactions arising from the charge and the solvent for ideal conditions

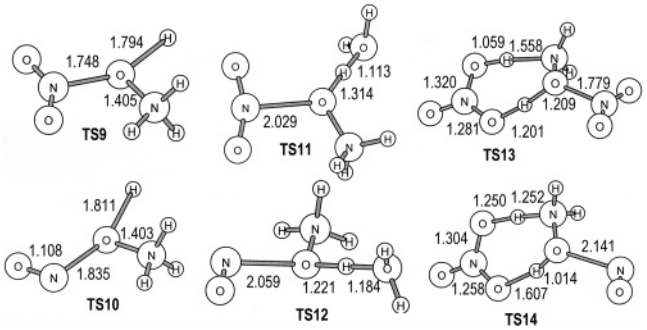

Figure 3. B3LYP/CBSB7/IEFPCM optimized geometries of ion−radical and ion−ion reactions leading to $NH_3ONO_2^+$ and NH_3ONO^+ intermediates. The value of bond length along the forming and breaking bonds in the reaction coordinate is given in angstroms.

corresponding to zero ionic strength. In a qualitative sense, these reactions are neither associative nor dissociative but are bimolecular reactions leading to two product molecules often referred to as interchange reactions. The electrostatic term involving charge and the solvent or the change in solvation pattern on forming the activated complex is expected to contribute little toward entropy of activation in solution as compared with the gas phase, $\Delta(\Delta S^{\ddagger}) \approx 0$, and the major contribution should come from change in internal modes of the reactant species. Similarly, the enthalpy of activation in solution $\Delta H^{\ddagger}_{soln}$ is larger than that in the gas phase for an ion−molecule reaction because of the charges, viz., the electrostatic term involving charge and solvent. We observe nearly the same qualitative trend in our TST results calculated from partition functions in solution. The rates of formation of intermediates are too slow, and consequently, ion−molecule pathways are not favorable (Table 4) for the formation of the reactive intermediates in solution.

Ion—Radical Reactions Involving Hydroxylammonium Ion (NH_3OH^+). Here

$$NH_3OH^+ + NO_2^{\bullet} \rightarrow NH_3ONO_2^+ + H^{\bullet} \quad (TS9) \qquad (28)$$

$$NH_3OH^+ + NO^{\bullet} \rightarrow NH_3ONO^+ + H^{\bullet} \quad (TS10) \qquad (29)$$

The transition states for these reactions are shown in Figure 3. Analysis of the eigenvector corresponding to the negative eigenvalue of the force constant matrix suggests the reaction coordinate to be an asymmetric stretch, viz., the cleavage of O−H bond and formation of O−N bond. The unprotonated hydroxylamine can be isomerized to the amineoxide $NH_3^+O^-$. This reaction is endothermic by 24.6 kcal/mol and has appreciable barrier ~50 kcal/mol in the gas phase. At the transition state, it appears that $NH_3^+O^-$ moiety of NH_3OH^+ is attracted toward $NO^{\bullet}$ and $NO_2^{\bullet}$ and the barrier arises from the bond energy of O−H bond in NH_3OH^+. However, as can be seen from Table 3, ion−radical reactions are extremely unlikely.

Ion—Ion Reactions Involving Hydroxylammonium Ion (NH_3OH^+). Here

$$NH_3OH^+ \cdot H_2O + NO_2^+ \rightarrow NH_3ONO_2^+ + H_3O^+ \quad (TS11) \qquad (30)$$

$$NH_3OH^+ \cdot H_2O + NO^+ \rightarrow NH_3ONO^+ + H_3O^+ \quad (TS12) \qquad (31)$$

The reactant NH_3OH^+ is complexed with the solvent water molecule via hydrogen bonding through its O−H bond with lone pair electrons of the oxygen in H_2O. Ion−ion reactions involve displacement of a proton between hydroxylammonium and water with the simultaneous bond formation between the attacking nitrosonium or nitronium ion with the oxygen of NH_3OH^+. Qualitatively, in these reactions, the activated complexes have a larger charge than either of the reactants and all three ionic species are solvated. However, the activated complex orientates the solvent considerably more than the reactant ions, and hence the entropy of activation decreases. As can be seen from Table 4, formation of intermediates is more favored through an ion−ion reaction as compared with the ion−molecule and ion−radical reactions discussed earlier. The optimized geometries of both the transition states are given in Figure 3 and the transition-state characteristics are tabulated in Table 4.

Ion−Molecule Reactions Involving the Complex, $NH_3OH\cdot NO_3$ (HAN). Here

$$HAN + NO_2^+ \rightarrow NH_3ONO_2^+ + HONO_2 \quad (TS13) \qquad (32)$$

$$HAN + NO^+ \rightarrow NH_3ONO^+ + HONO_2 \quad (TS14) \qquad (33)$$

The most stable structure of the complex HAN involves hydrogen bonding with both N−H and O−H bonds of NH_3OH with two oxygens of NO_3^-. The incoming NO^+ or NO_2^+ ion has the potential to form a complex with the oxygen lone pairs. The optimized geometries of the transition states are shown in Figure 3 and the transition-state characteristics are tabulated in Table 4 together with fitted rate parameters. The most favored pathway for the formation of the intermediates seems to be the reaction of NO^+/NO_2^+ with the HAN complex. The planar NO_3^- group in HAN provides the bridge for facile proton transfer. Interestingly, at 298 K, the rate constant for the formation of NH_3ONO^+ is nearly 2 orders of magnitude larger than that for $NH_3ONO_2^+$. Furthermore, as discussed in the Introduction for the equilibrium $HONO_2 + H^+ \rightleftharpoons H_2O + NO_2^+$, the concentration of NO_2^+ is much lower than that of NO^+ due to the small concentration of undissociated neutral nitric acid ($pK_a = -1.44$). Consequently, the intermediate for the scavenging reaction NH_3ONO^+ would form to a greater extent compared with the intermediate for the autocatalytic reaction, $NH_3ONO_2^+$, and the relative importance of reactions 32 and 33 depends also upon the equilibrium constant for the reaction, $HAN \rightleftharpoons NH_3OH^+ + NO_3^-$.

Ion—Molecule Reactions Involving Unprotonated Hydroxylamine (NH_2OH). Here

$$NH_2OH + NO_2^+ \rightarrow {}^+NH_2(NO_2)OH \qquad \Delta H_{gas}(298K) = -29.9 \text{ kcal/mol} \quad (34)$$

$$NH_2OH + NO_2^+ \rightarrow {}^+NH_2(ONO)OH \qquad \Delta H_{gas}(298K) = -33.9 \text{ kcal/mol} \quad (35)$$

$$NH_2OH + NO_2^+ \rightarrow NH_2O^+(NO_2)H \qquad \Delta H_{gas}(298K) = -14.2 \text{ kcal/mol} \quad (36)$$

$$NH_2OH + NO^+ \rightarrow {}^+NH_2(NO)OH \qquad \Delta H_{gas}(298K) = -33.1 \text{ kcal/mol} \quad (37)$$

$$NH_2OH + NO^+ \rightarrow NH_2O^+(NO)H \qquad \Delta H_{gas}(298K) = -20.0 \text{ kcal/mol} \quad (38)$$

Similar to protons, the NO^+ and NO_2^+ ions are capable of complexing with hydroxylamine using the lone pair of electrons on nitrogen or the oxygen. As observed in the case of PA, both in the gas and solution phase, the complexation is more favored at the nitrogen atom than at the oxygen atom of NH_2OH. However, the NO^+ and NO_2^+ binding enthalpies are consider-

ably smaller than the corresponding PAs. This is because at any given separation, the electrostatic energy released upon charge expansion from the free ion to the ion−neutral complex is considerably smaller for NO^+ and NO_2^+ than for H^+. Furthermore, H^+ is able to approach the nucleophilic center to a much shorter distance than NO^+ and NO_2^+. In solution, $^+NH_2(NO_2)OH$ and $^+NH_2(NO)OH$ are stabilized relative to $NH_2OH + NO^+/NO_2^+$ by approximately 27.4 and 19.2 kcal/mol. The importance of these pathways in autocatalytic and scavenging reactions depend on the relative concentration of unprotonated hydroxylamine, viz., the equilibrium constant of the equilibrium, $NH_3OH^+ \rightleftharpoons NH_2OH + H^+$, in acidic medium. The overall rate constants of these association reactions are diffusion limited.

Summarizing so far, the rate of formation of intermediates and their concentrations are controlled by the following equilibria:

$$NH_2OH + HONO_2 \rightleftharpoons HAN$$

$$HAN \rightleftharpoons NH_3OH^+ + NO_3^-$$

$$HONO_2 \rightleftharpoons H^+ + NO_3^-$$

$$HONO \rightleftharpoons H^+ + NO_2^-$$

$$HONO + H^+ \rightleftharpoons H_2O + NO^+$$

$$HONO_2 + H^+ \rightleftharpoons H_2O + NO_2^+$$

$$NH_2OH + H^+ \rightleftharpoons NH_3OH^+$$

$$NO^+ + NO_3^- \rightleftharpoons N_2O_4 \rightleftharpoons 2NO_2^\bullet$$

$$NO^+ + NO_2^- \rightleftharpoons N_2O_3 \rightleftharpoons NO^\bullet + NO_2^\bullet$$

and reaction sequences

$$NH_3OH^+\cdot H_2O + NO_2^+ \rightarrow NH_3ONO_2^+ + H_3O^+$$

$$NH_3OH^+\cdot H_2O + NO^+ \rightarrow NH_3ONO^+ + H_3O^+$$

$$HAN + NO_2^+ \rightarrow NH_3ONO_2^+ + HONO_2$$

$$HAN + NO^+ \rightarrow NH_3ONO^+ + HONO_2$$

The importance of the intermediate $NH_3ONO_2^+$ depends on the available concentration of NO_2^+ in the reaction medium.

Formation of HNO in the Autocatalytic Reaction via the Decomposition of the Intermediate $NH_3ONO_2^+$ and NH_3ONO^+. The formation of HNO was suggested as a slow reaction (reaction 9) in Stedman mechanism.[8] One possible pathway for the formation of HNO consists of three elementary steps: (a) formation of $NH_3ONO_2^+$, (b) its deprotonation from the nitrogen site, and (c) reprotonation at the oxygen site with simultaneous O−N bond cleavage.

$$NH_3ONO_2^+ + H_2O \rightarrow NH_2ONO_2 + H_3O^+ \quad (39)$$

$$NH_2ONO_2 + H_3O^+ \xrightarrow{TS15} NH_2O^+ + HONO + H_2O \quad (40)$$

Many attempts were made to find the five membered transition states for the synchronous 1,4- H migration in NH_2ONO_2 and as well in $NH_3ONO_2^+$ without success. The most promising route is the attack of a proton at the oxygen end of the nitro group in NH_2ONO_2. Optimized transition state is shown in Figure 4, and the transition state characteristics are tabulated in Table 5. It must be stated, however, that the concentration of NO_2^+ in the medium is very small; consequently, it is unlikely for the HNO formation to proceed through $NH_3ONO_2^+$ intermediate.

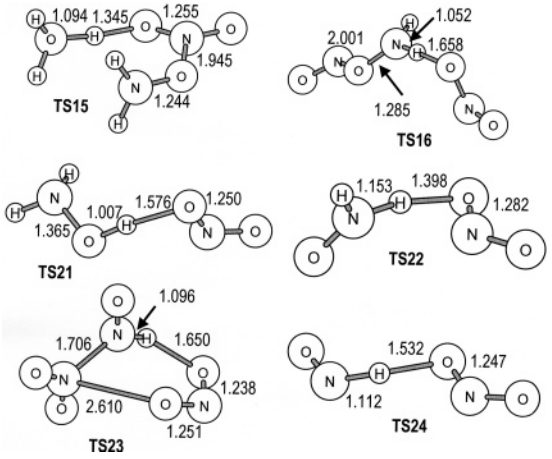

Figure 4. B3LYP/CBSB7/IEFPCM optimized geometries of transition states leading to the formation of HNO and HONO from $NH_3ONO_2^+$ and NH_3ONO^+ intermediates and as well from NH_2OH. The value of bond length along the forming and breaking bonds in the reaction coordinate is given in angstroms.

TABLE 5: B3LYP/CBSB7/IEFPCM Barrier Heights in Solution Phase, Magnitude of the Imaginary Frequency, Value of the Rate Constant (cm^3/(mol s)) at 298.15 K, and the Modified Arrhenius-Fitted Parameters for the Formation of HNO from $NH_3ONO_2^+$ and NH_3ONO^+ Intermediates and H-Abstraction Pathways in Aqueous Solution

reacn	E_0(soln)	ν(soln)	k(soln)(298K)	A	n	E_a/R
40	21.6	184*i*	8.67E−5	2.33E7	1.61	10 580
41	14.8	590*i*	6.65E1	1.61E5	2.73	7036
42	41.8	904*i*	2.9E−20	4,6E5	1.85	20 430
43	31.3	904*i*	6.5E−13	2.5E2	2.84	14 830
44	34.8	1805*i*	5.61E−18	3.9E2	1.81	16 690
45	41.1	1066*i*	1.34E−21	2.8E4	1.46	19 850
46	7.9	896*i*	3.06E5	2.64E5	1.97	3294
47	4.8	629i	6.55E5	6.88E2	2.11	1632
48	3.9	474i	3.61E6	1.37E3	2.06	668.8
49	15.6	1066i	3.01	2.19E5	2.08	2416

Another possible pathway is via the NH_3ONO^+ intermediate by the loss of a proton to a solvent molecule followed by hydrogen abstraction from NH_2ONO by $NO_2^\bullet$.

$$NH_2ONO + NO_2 \xrightarrow{TS16} HONO + HNO + NO \quad (41)$$

The transition state for hydrogen abstraction is depicted in Figure 4. The rate of this bimolecular hydrogen abstraction is relatively slow compared with the competitive unimolecular reaction channels starting from NH_2ONO. Unimolecular reactions of NH_2ONO will be discussed under the section of scavenging reaction pathways. However, this pathway could be important in the autocatalytic mechanism at high NH_3OH^+ concentrations. Under this condition, the scavenging reaction would become dominant over autocatalytic since most of NH_3OH^+ would exist as NH_3ONO^+ and the unimolecular isomerization (as shown below) from O-nitrosation (NH_2ONO) to N-nitrosation ($NH_2(NO)O$) is faster than the bimolecular reaction rate with NO_2 radical.

Autocatalytic Reaction Pathways without the Involvement of $NH_3ONO_2^+$ or NH_3ONO^+ Intermediate. In our systematic investigation, we also explored the possibilities of simple hydrogen abstraction steps leading to HNO. The elementary steps involved in these pathways are

$$NH_3OH^+ + NO_2^\bullet \xrightarrow{TS17} NH_3O^+ + HONO \quad (42)$$

$$NH_3OH^+ + NO_2^\bullet \xrightarrow{TS18} NH_2OH^+ + HONO \quad (43)$$

$$NH_3O^+ + NO_2^\bullet \xrightarrow{TS19} NH_2O^+ + HONO \rightarrow HNO + H^+ + HONO \quad (44)$$

$$NH_2OH^+ + NO_2^\bullet \xrightarrow{TS20} NH_2O^+ + HONO \rightarrow HNO + H^+ + HONO \quad (45)$$

$$NH_2OH + NO_2^\bullet \xrightarrow{TS21} NH_2O^\bullet + HONO \quad (46)$$

$$NH_2O^\bullet + NO_2^\bullet \xrightarrow{TS22} HNO + HONO \quad (47)$$

As can be seen from Table 5, ion−radical reactions are extremely unlikely. The Cartesian coordinates of ion−radical transition states are provided as a supplementary table. The most favorable pathway for HNO formation seems to be from the unprotonated hydroxylamine via successive hydrogen abstraction by two NO_2 radicals. This is in agreement with the earlier proposition from Pembridge and Stedman.[8] The rate of autocatalytic reaction will therefore depend on the available unprotonated hydroxylamine concentration and NO_2 radical. Experimentally, with increased [$HONO_2$], the rate constant for autocatalytic generation of nitrous acid decreases slightly and is probably due to the decreased [NH_2OH] at high acid strengths.

HNO once formed can react with another molecule of dinitrogen tetroxide or can transfer its hydrogen atom, via hydrogen abstraction, to $NO_2^\bullet$. Both processes have been considered in the present work (see Figure 4), and the kinetic parameters are included in Table 5. We found molecular elimination to be more favorable than radical abstraction.

$$HNO + N_2O_4 \xrightarrow{TS23} HONO + N_2O_3 \quad (48)$$

$$HNO + NO_2^\bullet \xrightarrow{TS24} HONO + NO^\bullet \quad (49)$$

$$NO^\bullet + NO_2^\bullet \rightarrow N_2O_3 \quad (50)$$

In summary, according to our calculations, the series of elementary steps involved in the mechanism of autocatalytic reaction of hydroxylamine are as follows:

$$HONO_2 \rightleftharpoons H^+ + NO_3^-$$

$$HONO + H^+ \rightleftharpoons NO^+ + H_2O$$

$$NO^+ + NO_3^- \rightleftharpoons N_2O_4$$

$$N_2O_4 \rightleftharpoons 2NO_2^\bullet$$

$$NH_2OH + H^+ \rightleftharpoons NH_3OH^+$$

$$NH_2OH + NO_2^\bullet \rightarrow NH_2O^\bullet + HONO$$

$$NH_2O^\bullet + NO_2^\bullet \rightarrow HONO + HNO$$

$$HNO + N_2O_4\,(2NO_2^\bullet) \rightarrow HONO + N_2O_3$$

$$N_2O_3 + H_2O \rightarrow 2HONO$$

The schematic potential energy surface of these reactions is shown in Figure 5. In addition to this major channel, a minor contribution could be expected from NH_3ONO^+ and $NH_3ONO_2^+$ intermediates as well

$$NH_3OH^+\cdot H_2O + NO^+ \rightarrow NH_3ONO^+ + H_3O^+$$

$$NH_3OH^+\cdot H_2O + NO_2^+ \rightarrow NH_3ONO_2^+ + H_3O^+$$

$$NH_3OH^+ + NO_3^- \rightleftharpoons HAN$$

$$HAN + NO^+ \rightarrow NH_3ONO^+ + HONO_2$$

$$HAN + NO_2^+ \rightarrow NH_3ONO_2^+ + HONO_2$$

$$NH_3ONO^+ + H_2O \rightarrow NH_2ONO + H_3O^+$$

$$NH_2ONO + NO_2 \rightarrow HONO + HNO + NO$$

$$NH_2ONO_2 + H_3O^+ \rightarrow NH_2O^+ + HONO + H_2O$$

$$NO + NO_2 \rightarrow N_2O_3$$

$$N_2O_3 + H_2O \rightarrow 2HONO$$

Decomposition of the Intermediate NH_3ONO^+ to N_2O and H_2O: PES for the Scavenging Reaction. The following reaction sequence is considered for scavenging based on available literature data.

$$NH_3ONO^+ \rightarrow NH_2ONO \quad (51)$$

$$NH_2ONO \xrightarrow{TS25} H_2N(NO)O \quad (52)$$

$$NH_2ONO\cdot 2H_2O \xrightarrow{TS25'} H_2N(NO)O\cdot 2H_2O \quad (53)$$

$$H_2N(NO)O \xrightarrow{TS26} NH(NO)OH \quad (54)$$

$$H_2N(NO)O\cdot 2H_2O \xrightarrow{TS26'} NH(NO)OH \quad (55)$$

$$NH(NO)OH \xrightarrow{TS27} HONNOH \quad (56)$$

$$HN(NO)OH \xrightarrow{TS29} N_2O + H_2O \quad (57)$$

$$HONNOH \xrightarrow{TS28} N_2O + H_2O \quad (58)$$

$$NH(NO)OH \xrightarrow{H^+} HNNO^+ + H_2O \quad (59)$$

$$HNNO^+ + H_2O \rightarrow N_2O + H^+ + H_2O \quad (60)$$

Optimized geometries of transition states TS25 and TS26 are shown in Figure 6. The transition states TS25 and TS26 were obtained both in the presence and in the absence of explicit water molecules. It should be pointed out from the outset that in IEFPCM calculations one is mainly focusing on the electrostatic interactions between the solvent (bulk water) and the reacting system and does not consider explicit hydrogen bonding between water and the reacting system. The neglect of the role of isolated water molecules could lead to a predicted mechanism that might be too different from the real processes taking place in solution. To address this issue, two extra water molecules were added to the reaction of 1,2-H and 1,2-NO migrations (TS25′ and TS26′). Explicit water molecules have been shown[27] to influence the barrier height for the 1,2-proton migration in $NH_2OH_2^+ \rightarrow NH_3OH^+$. Similary, 1,2-H migration is favored by the inclusion of explicit water molecules. The barrier heights for these reactions are computed as the energy difference between the complex $NH_2ONO\cdot 2H_2O$ (or $H_2N(NO)O\cdot 2H_2O$) and the corresponding transition states with the assumption that the basis set superposition error (BSSE) effects, which are present in reactants and in the TS, nearly compensate each other.

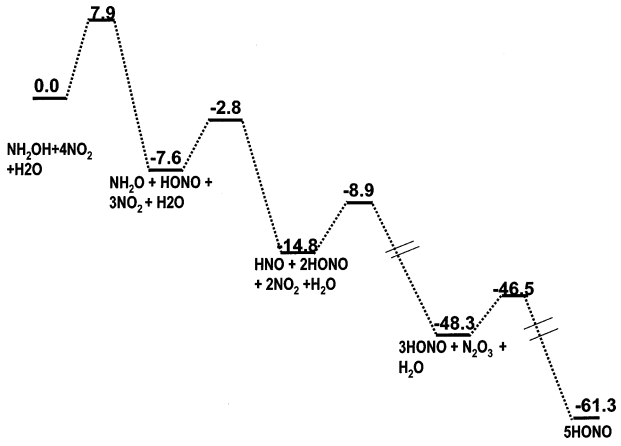

Figure 5. B3LYP/CBSB7/IEFPCM schematic potential energy surface for the free radical pathway leading to autocatalytic generation of HONO in reactions of hydroxylamine with nitric acid. Relative energies are given in kcal/mol.

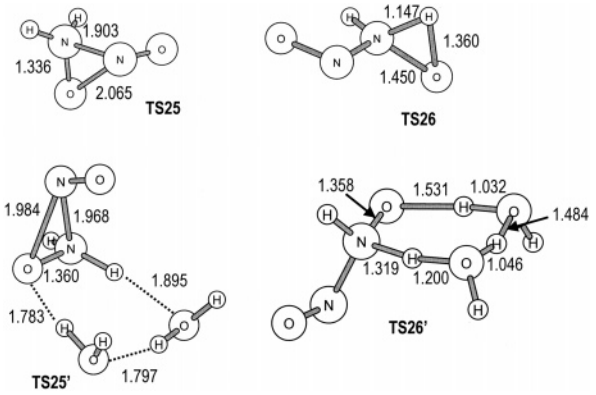

Figure 6. B3LYP/CBSB7/IEFPCM optimized geometries of isomerization transition states of the intermediates involved in the scavenging reaction, with and without explicit solvent water molecules. The value of the bond length along the forming and breaking bonds in the reaction coordinate is given in angstroms.

TABLE 6: B3LYP/CBSB7/IEFPCM Barrier Heights in Solution Phase, Magnitude of the Imaginary Frequency, Value of the Rate Constant (cm^3/(mol s)) at 298.15 K, and the Modified Arrhenius-Fitted Parameters for the Reactions Involved in the Scavenging Reaction of HONO by NH_3OH

reacn	E_0(soln)	ν(soln)	k(soln)(298K)	A	n	E_a/R
52	17.6	198*i*	0.52	1.37E12	0.22	8889
53	13.2	195*i*	9.81	9.1E8	0.72	6690
54	34.9	1668*i*	0.14E−12	3.90E9	0.78	4330
55	9.99	1083*i*	1.32E5	1.92E12	−0.32	4603
56	8.6	3150*i*	2.44E8	1.16E14	−0.29	4114
57	59.3	1822*i*				
58	20.1	1206*i*	5.52E−2	7.8E12	−0.05	9883

It is interesting to notice that the second water molecule acts as a catalyst, whereby it abstracts a hydrogen from the amino group of $NH_2(NO)O$ and donates another hydrogen to the oxygen of nitrosoamineoxide (Figure 6). The transition-state structure involves a seven-membered ring which contains the two water molecules and the H−N−O moiety of $NH_2(NO)O$. Comparing the results in the presence and absence of explicit water molecules, it is clear that the intrinsic barrier corresponding to the hydrogen transfer decreases (Table 6) significantly with explicit water molecules. The decrease in the barrier is mainly due to a change in the mechanism as a result of hydrogen bonding of the water moiety to the substrate.

NH(NO)OH can either undergo further protonation, 1,3-H migration leading to hyponitrous acid via TS27 (Figure 7) or 1,1-elimination of H_2O via TS29 (Figure 7). The barrier for

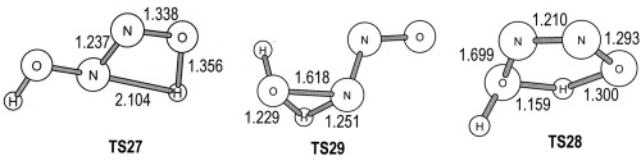

Figure 7. B3LYP/CBSB7/IEFPCM optimized geometries of decomposition transition states leading to N_2O formation from hyponitrous acid and NH(NO)OH. The value of the bond length along the forming and breaking bonds in the reaction coordinate is given in angstroms.

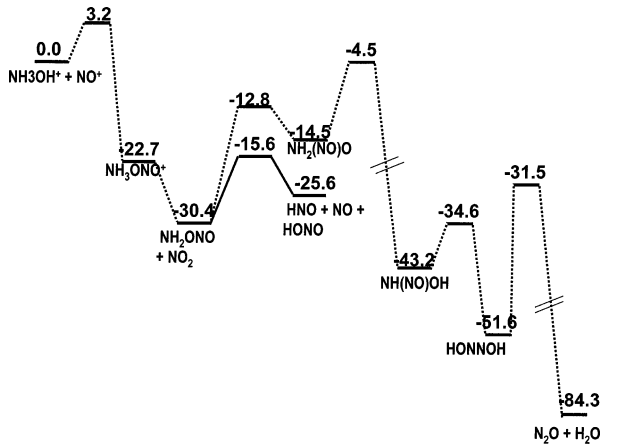

Figure 8. B3LYP/CBSB7/IEFPCM schematic potential energy surface for the unimolecular reaction involved in the scavenging pathway. The solid line represents the bimolecular reaction, and it connects the pathway originating from NH_2ONO and leading to the autocatalytic reaction. Relative energies are given in kcal/mol.

H-migration is rather small, and one would expect a competitive protonation and H-migration from NH(NO)OH. The barrier for elimination is quite high and therefore an elementary step proceeding through TS29 is less likely. We also investigated the formation of N_2O from hyponitrous acid via 1,3- elimination of water (TS28) (Figure 7). However, the barrier height for elimination is ∼21 kcal/mol. This is in contradiction to the proposition by Stedman and co-workers to be a fast step. Bennett et al.[6] has postulated hyponitrous acid to be an intermediate to explain the formation of N_2 as one of the reaction products at high acid strength and low hydroxylamine concentrations. HONNOH once formed could undergo competitive protonation or nitrosation depending upon the concentration of NH_3OH^+ and the ionic strength. At low concentrations of $[NH_3OH^+]$, as proposed by Bennett et al., nitrous acid will get protonated leading to the formation of NO^+, which then reacts with HONNOH to form N_2.

$$HONO + H^+ \rightleftharpoons H_2O + NO^+$$

$$NO^+ + HONNOH \rightarrow HONNONO + H^+ \rightarrow NO_2 + OH + N_2$$

Otherwise, it would undergo further protonation leading to N_2O.

$$HONNOH + H^+ \rightarrow HONN^+ + H_2O \rightarrow N_2O + H^+$$

Consequently, the rate-determining step in the scavenging mechanism is the formation of nitrosoamineoxide ($H_2N(NO)O$). The calculated rate constant for this step is in agreement with the experimentally determined overall scavenging rate constant. The schematic PES for the scavenging reaction computed at the B3LYP/CBSB7/IEFPCM level is shown in Figure 8. In summary, scavenging reaction proceeds through the NH_3ONO^+ intermediate and the rate-determining step is the isomerization

of O-nitrosated hydroxylamine (NH_2ONO) to N-nitrosated hydroxylamine $NH_2(NO)O$. Both hyponitrous acid and NH(NO)OH would preferably undergo further protonation, leading to loss of water and formation of N_2O.

Conclusions

Reaction pathways of the decomposition of hydroxylamine in the presence of nitrous and nitric acids were studied in solution phase using ab initio molecular orbital calculations. Stationary points, including 29 transition states associated with ion−molecule, ion−radical, and ion−ion reactions, were successfully located and characterized by employing hybrid DFT procedures at the B3LYP/CBSB7/IEFPCM level without any restriction on the internal coordinates. The gas-phase and aqueous thermochemistry have been calculated for about 45 $H_xN_yO_z$ species. The computed parameters are in good agreement with the available experimental data. The calculated values for the best-established free energy changes in solution, those of HONO, $HONO_2$, and NH_3OH^+ show larger differences. These differences are consistent with the fact that we are not including any direct solvent interactions (predominantly hydrogen bonding) to the neutrals or anions. The kinetic parameters needed for the modeling of the decomposition of hydroxylamine are obtained via transition-state theory calculations and, wherever possible, the calculated rate parameters are discussed in comparison with the experimental value. The reaction of nitrous acid with hydroxylamine in acidic nitrate solutions follows the reaction schemes outlined by earlier workers and proceeds through O- and N-nitrosated intermediates while the autocatalytic reaction proceeds through a free radical pathway from unprotonated NH_2OH and as well from NH_2ONO. The importance of the role of intermediates NH_3ONO^+ and $NH_3ONO_2^+$ in autocatalytic mechanism needs to be established from modeling results using the ab initio computed thermochemical and kinetic parameters. Since ionic interactions are significant in electrolyte solutions, reactions involving charges will occur under grossly nonideal conditions. The ideal equilibrium constant for the formation of the activated complex is related to the nonideal one by

$$K^{\ddagger *}_{\text{non-ideal}} = K^{\ddagger *}_{\text{ideal}}\left(\frac{\gamma_A\gamma_B}{\gamma^{\ddagger}_{AB}}\right)$$

In the future, it will be interesting to calculate the activity coefficient of all ionic species using the COSMO-RS[26] approach. To our knowledge, the performance of COSMO-RS has so far not been tested in the literature for strong electrolytes such as HNO_3 or the salt HAN. Such a work could be significant for the sophisticated COSMO-RS approach because extensive experimental data are available for the activity coefficient of nitric acid and mixtures of nitric acid and HAN. Work is in progress to theoretically compute the activity coefficients of all ionic species using the COSMO screening charge densities. The rigorous ab initio SCRF results reported here should be regarded as an initial step toward better understanding the reactivity of NH_2OH, HONO, and $HONO_2$. Use of explicit water molecules in our system enhances the rate constant for unimolecular isomerization reactions. However, additional work must be done to better understand the size of the solvation shell and the physics behind the specific number of solvent molecules in the shell.

Supporting Information Available: A table of B3LYP/CBSB7 optimized Cartesian coordinates of the transition states corresponding to ion−radical reactions involving the hydroxylammonium ion. This material is available free of charge via the Internet at http://pubs.acs.org.

References and Notes

(1) Orth, D. A.; McKibben, J. M.; Scotten, W. C. *Proceedings of the International Solvent Extraction Conference*; Society Chemical Industry: London, 1971; p 514.
(2) Dukes, E. K. *J. Am. Chem. Soc.* **1960**, *82*, 9.
(3) Hughes, M. N.; Stedman, G. *J. Chem. Soc.* **1963**, 2824.
(4) Morgan, T. D. B.; Stedman, G.; Hughes, M. N. *J. Chem. Soc. B* **1968**, 344.
(5) Bothner-By, A.; Friedman, L. *J. Chem. Phys.* **1952**, *20*, 459.
(6) Bennett, M. R.; Brown, G. M.; Maya, L.; Posey, F. A. *Inorg. Chem.* **1982**, *21*, 2461.
(7) Gowland, R. J.; Stedman, G. *J. Inorg. Nucl. Chem.* **1981**, *43*, 2859.
(8) Pembridge, J. R.; Stedman, G. *J. Chem. Soc., Dalton Trans.* **1979**, 1657.
(9) Gowland, R. J.; Stedman, G. *J. Chem. Soc., Chem. Commun.* **1983**, 1038.
(10) Longstaff, J. V. L.; Singer, K. *J. Chem. Soc.* **1954**, 2610.
(11) Frisch, M. J. T.; G. W.; Schlegel, H. B.; Scuseria, G. E.; Robb, M. A.; Cheeseman, J. R.; Montgomery, J. A., Jr.; Vreven, T.; Kudin, K. N.; Burant, J. C.; Millam, J. M.; Iyengar, S. S.; Tomasi, J.; Barone, V.; Mennucci, B.; Cossi, M.; Scalmani, G.; Rega, N.; Petersson, G. A.; Nakatsuji, H.; Hada, M.; Ehara, M.; Toyota, K.; Fukuda, R.; Hasegawa, J.; Ishida, M.; Nakajima, T.; Honda, Y.; Kitao, O.; Nakai, H.; Klene, M.; Li, X.; Knox, J. E.; Hratchian, H. P.; Cross, J. B.; Bakken, V.; Adamo, C.; Jaramillo, J.; Gomperts, R.; Stratmann, R. E.; Yazyev, O.; Austin, A. J.; Cammi, R.; Pomelli, C.; Ochterski, J. W.; Ayala, P. Y.; Morokuma, K.; Voth, G. A.; Salvador, P.; Dannenberg, J. J.; Zakrzewski, V. G.; Dapprich, S.; Daniels, A. D.; Strain, M. C.; Farkas, O.; Malick, D. K.; Rabuck, A. D.; Raghavachari, K.; Foresman, J. B.; Ortiz, J. V.; Cui, Q.; Baboul, A. G.; Clifford, S.; Cioslowski, J.; Stefanov, B. B.; Liu, G.; Liashenko, A.; Piskorz, P.; Komaromi, I.; Martin, R. L.; Fox, D. J.; Keith, T.; Al-Laham, M. A.; Peng, C. Y.; Nanayakkara, A.; Challacombe, M.; Gill, P. M. W.; Johnson, B.; Chen, W.; Wong, M. W.; Gonzalez, C.; Pople, J. A. GAUSSIAN03, Revision C.02 ed.; Gaussian Inc.: Wallingford CT, 2004.
(12) Montgomery, J. A., Jr.; Frisch, M. J.; Ochterski, J. W.; Petersson, G. A. *J. Chem. Phys.* **2000**, *112*, 6532.
(13) Nicolaides, A.; Rauk, A.; Glukhovtsev, M. N.; Radom, L. *J. Phys. Chem.* **1996**, *100*, 17460.
(14) Petersson, G. A.; Malick, D. K.; Wilson, W. G.; Ocherski, J. W.; Montgomery, J. A., Jr.; Frisch, M. J. *J. Chem. Phys.* **1998**, *109*, 10570.
(15) Mennucci, B.; Tomasi, J. *J. Chem. Phys.* **1997**, *106*, 5151.
(16) Sumathi, R.; Carstensen, H.-H.; Green, W. H.; Jr. *J. Phys. Chem. A* **2001**, *105*, 6910.
(17) Hirschfelder, J. O.; Wigner, E. *J. Chem. Phys.* **1939**, *93*, 1761.
(18) Angelelli, F.; Aschi, M.; Cacace, F.; Pepi, F.; de Petris, G. J. *J. Phys. Chem.* **1995**, *95*, 6551.
(19) Ishikawa, Y.; R. C.; B. J. *Chem. Phys. Lett.*, **2001**, *338*, 353.
(20) Sunderlin, L. S.; Squires, R. R. *Chem. Phys. Lett.* **1993**, *222*, 333.
(21) Dixon, D. A.; Feller, D.; Zhan, C.-G.; Francisco, J. S. *Int. J. Mass Spectrosc.* **2003**, *227*, 421.
(22) Schwartz, S. E.; White, W. H. In *Advances in Environmental Science and Technology*; Nriagu, J. O., Ed.; John Wiley & Sons: New York, 1983; Vol. 12.
(23) Park, J.-Y.; Lee, Y.-N. *J. Phys. Chem.* **1988**, *92*, 6294.
(24) Schmid, G.; Bahr, G. *Z. Phys. Chem.* **1964**, *41*, 8.
(25) Abel, E.; Schmid, H. *Z. Phys. Chem.* **1928**, *186*, 430.
(26) Barney, G. S.; Vial, M. A. DCS01-RRJ-DS-CAL-H-35613-A, DOE Report; Department of Energy: Washington, DC, 2005.
(27) Marquez, M.; Mari, F.; Gonzales, C. A. *J. Phys. Chem. A* **1999**, *103*, 6191.
(28) Taken from: http://webbook.nist.gov.